journal of the mechanical behavior of biomedical materials 140 (2023) 105700

Contents lists available at ScienceDirect

Journal of the Mechanical Behavior of Biomedical Materials

journal homepage: www.elsevier.com/locate/jmbbm

Evaluation of innovative polyvinyl alcohol/ alginate/ green palladium nanoparticles composite scaffolds: Effect on differentiated human dental pulp stem cells into osteoblasts

Enas Ismail [a,b,*], Mostafa Mabrouk [c,**], Zeinab A. Salem [d,e], Nermeen AbuBakr [d,f], Hanan Beherei [c]

[a] Department of Restorative Dentistry, Faculty of Dentistry, University of the Western Cape, Parow, 7505, Cape Town, South Africa
[b] Physics Department, Faculty of Science, Girl's Branch, Al Azhar University, Nasr City, Cairo, Egypt
[c] Refractories, Ceramics, and Building Materials Department, National Research Centre, 33El Bohouthst, Dokki, Giza, Egypt
[d] Department of Oral Biology, Faculty of Dentistry, Cairo University, Cairo, P.O 11553, Egypt
[e] Faculty of Oral and Dental Medicine, Ahram Canadian University, 6 October City, P.O 12573, Egypt
[f] Stem Cells and Tissue Engineering Unit, Faculty of Dentistry, Cairo University, Cairo, P.O 11553, Egypt

ARTICLE INFO

Keywords:
3D scaffold
Polymer hybrids
Green Pd NPs
Aspalathus linearis extract
Dental pulp stem cells
Osteoblasts

ABSTRACT

Three-dimensional (3D) scaffolds are attracting great concern for bone tissue engineering applications. However, selecting an appropriate material with optimal physical, chemical, and mechanical properties is considered a great challenge. The green synthesis approach is essential to avoid the production of harmful by-products through textured construction, sustainable, and eco-friendly procedures. This work aimed at the implementation of natural green synthesized metallic nanoparticles for the development of composite scaffolds for dental applications. In this study, innovative hybrid scaffolds of polyvinyl alcohol/alginate (PVA/Alg) composite loaded with various concentrations of green palladium nanoparticles (Pd NPs) have been synthesized. Various characteristic analysis techniques were used to investigate the synthesized composite scaffold's properties. The SEM analysis revealed impressive microstructure of the synthesized scaffolds dependent on the Pd NPs concentration. The results confirmed the positive effect of Pd NPs doping on the sample stability over time. The synthesized scaffolds were characterized by the oriented lamellar porous structure. The results confirmed the shape stability, without pores breakdown during the drying process. The XRD analysis confirmed that doping with Pd NPs does not affect the crystallinity degree of the PVA/Alg hybrid scaffolds. The mechanical properties results (up to 50 MPa) confirmed the remarkable effect of Pd NPs doping and its concentration on the developed scaffolds. The MTT assay results showed that the incorporation of Pd NPs into the nanocomposite scaffolds is necessary for increasing cell viability. According to the SEM results, the scaffolds with Pd NPs provided the differentiated grown osteoblast cells with enough mechanical support and stability and the cells had a regular form and were highly dense. In conclusion, the synthesized composite scaffolds expressed suitable biodegradable, osteoconductive properties, and the ability to construct 3D structures for bone regeneration, making them a potential option for treating critical deficiencies of bone.

1. Introduction

Bone damage is one of the main issues in the oral cavity. It occurs due to some infections, trauma, or other multifactorial causes. As a result, they may cause some functional or esthetical problems. Surgical intervention is a common procedure for mandibular bone defect treatment. It is well recognized that mandibular discontinuities may result in inadequate assistance for the suprahyoid muscles. Reconstruction of the cosmetic and functional deformities enhances the life quality of the patient. In the last decade, surgical techniques have improved considerably. However, reconstruction of large bone fractures in the lower jaw remains a major challenge in maxillofacial re-treatment (Brierly et al.,

* Corresponding author. Department of Restorative Dentistry, Faculty of Dentistry, University of the Western Cape, Parow, 7505, Cape Town, South Africa.
** Corresponding author.
E-mail addresses: 4270789@myuwc.ac.za, enas.ismail4@yahoo.com (E. Ismail), mostafamabrouk.nrc@gmail.com (M. Mabrouk).

https://doi.org/10.1016/j.jmbbm.2023.105700
Received 11 December 2022; Received in revised form 29 January 2023; Accepted 30 January 2023
Available online 9 February 2023

2016). To reconstruct these defects, autogenous bone (AB) grafting was deemed. However, the sources of donor tissues are restricted. In contrast, the use of autografts was not a good bone replacement due to antigens that induce the immune response and risks associated with infection (Marthy and Richter, 1998). Then, allografts (synthetic biomaterials) have extensively been covered as prospective bone replacements. However, a deficiency of osteoblasts, osteogenesis, and limited new bone formation occurs after bone conduction is achieved (Jang et al., 2012). Hence, a combination of biomaterials and tissue engineering based on autologous stem cells revealed a promising discovery of its use as a promising alternative method (Pittenger et al., 1999).

Characterizing dental pulp stem cells (DPSCs) attracted great attention in applications of regenerative biomedicine (Tatullo et al., 2015). The DPSCs are contemplated as an autologous cell source, and they can be obtained from removed teeth. DPSCs have demonstrated good osteogenic differentiation capacity in vitro and in vivo studies (Lindroos et al., 2008). Some reports have revealed the effective combination of DPSCs with 3D biomaterial scaffolds in the production of solid bone-like tissues (d'Aquino et al., 2008). Moreover, selecting the constituents of biomaterial scaffolds is very critical as they are responsible for the scaffolds-cells interactions. Previous reports have focused on the utilization of synthetic polymers such as poly (vinyl alcohol) (PVA) as a matrix for inorganic fillers for the bone regeneration process (Sordi et al., 2021). Synthetic polymer matrices have characterized structure, dependable material sources, long periods of usability, diminished danger of immunogenicity, and might be produced in enormous amounts with reproducibility. The fundamental impediments are their low bioactivity, corrosive side-effects, and acid by-products, which offer no natural environments to cells (Ruedinger et al., 2015). In this way, synthetic polymer matrices may be combined with natural materials such as polysaccharides to remunerate those disadvantages (Sordi et al., 2021). Alginate (Alg) is an unbranched anionic polysaccharide made of various quantities of (1 → 4)- linked β-d-mannuronic acid and α-l-guluronic acid build-ups and usually originated from brown seaweed. Alg can frame a polymer matrix scaffold under gentle conditions with multivalent metal cations, such as Ba^{2+}, Ca^{2+}, Zn^{2+}, Sr^{2+}, and other cations as well (Lee and Mooney, 2012; Treenate and Monvisade, 2017; Gombotz and Wee, 2012). The presence of calcium salts causes a frame calcium alginate gel which would enhance the bioactivity of the resultant gel. Furthermore, alginate likewise possesses benefits including being easily located, non-harmful, cheap, biocompatible, and simple to frame scaffold shape (Han et al., 2013).

Furthermore, nanoparticles are vital for biomedical implementations including composite structures for bone recovery as they have impressive restorative, antibacterial, and antioxidant properties owed to the higher surface area to volume proportions contrasted with the bulky state. Therefore, a few scientific groups have developed these metallic nanoparticles through green eco-friendly techniques (Kiani et al., 2020). Among various metallic nanoparticles, palladium nanoparticles (Pd-NPs) have exhibited different potentialities in various biomedical applications such as biosensors, and nano-carriers for the delivery of medications. This encourages scientific groups to diminish the expense and harmfulness of Pd-NPs, to increase their multi-functionality (Ahmadi et al., 2019; Phan et al., 2020; Shanthi et al., 2015; He et al., 2021). Hence, fabricated porous novel Alg/PVA/Pd NPs hydrogel composite scaffolds were synthesized through the freeze-drying method. The physical, mechanical, chemical, and cellular behaviours of Alg/PVA/Pd-NPs scaffolds were investigated. Furthermore, dental stem cell (DSCs) studies (cell growth, cell attachment, and cell proliferation along with differentiation into osteoblast cells) were assessed in the presence of the fabricated scaffolds.

2. Materials and methods

2.1. Materials

The chemicals used were of strict standard and Agrade, and obtained from an international chemistry Co. Ltd. The chemicals were used as received without further purification. Palladium II chloride, (Mwt177.33 g/mol, 99.999% (Aldrich, South Africa) and dried *Aspalathus Linearis* leaves were used as the main precursors for the green synthesis of Pd NPs. The *Aspalathus Linearis* plant material was freshly dried and obtained through the S.A. Rooibos Council in South Africa. Sodium alginate CAS:9005-38-3 delivered by Fisher Scientific, UK, and PVA of molecular weight 13,000–23,000, purchased from Sigma Aldrich, USA.

2.2. Green synthesis of Pd NPs

The green synthesis process for the selected Pd NPs was carried out via the aqua extraction process of *Aspalathus linearis*. The *Aspalathus Linearis* natural plant, commonly called rooibos tea, can effectively work as a reducing agent as well as a chelating agent in the formation of Pd NPs. This is attributed to its highly bioactive compounds such as Aspalathin, Nothofagin, and other polyphenolic compounds (Krafczyk and Glomb, 2008). The extraction of the polyphenol compounds from the fermented Rooibos tea was done based on our previous work, Ismail et al., 2017 (Ismail et al., 2017a). In practice, a gram of *Aspalathus Linearis* dried leaves was added to 50 mL of deionized water for 20min at 70 °C to enhance the aqua extraction process, and the color changes into deep orange/brown were observed. To obtain a pure natural extract, a filtration process was carried out three times. For the biosynthesis process of Pd NPs, Palladium II chloride was used as the main Pd precursor. A stock concentration of 10^{-2} M of Palladium II chloride left under continues stirring for 15min at room temperature to ensure complete dissolving of the precursor. Then, it was added to the previously prepared *Aspalathus linearis* natural extract. The mixture was left over to react for 30min. to complete the oxidation/reduction process. A change in color into dark brown is an initial indication of Pd NPs formation. Palladium ions were reduced via the green chemistry approach using Rooibos extract as a reducing/chelating agent. The solution was left to dry at ~90 °C for 1h, in an atmospheric condition. This is to ensure removing of any excess water and bio-compounds.

2.3. Preparation of Alg/PVA/Pd NPs scaffolds

Stock solutions of sodium alginate (Alg) and PVA (20% $^{W}/_{V}$) were prepared through the aqueous dissolving of the used polymers. The solutions were stirred at 80 °C for 1h and to prepare three composite scaffolds containing the eco-friendly fabricated Pd, (1, 2, and 4 ml) were added to the (18 ml) stoke solution of solubilized polymers. Then the obtained solutions were kept stirring overnight. The above mixtures were cast into 24 well plates and were further, frozen and freeze dried at −56 °C for 24h. Then, the synthesized scaffolds were immersed in a 0.5M solution of $CaCl_2$ for 20 min for cross-linking. After obtaining the scaffolds, it was rinsed with distilled water for three times and left to dry at normal room temperature for further investigations.

2.4. Characterization techniques

2.4.1. Morphological structure

Transmission Electron Microscopy (TEM) is an ideal technique for identifying the size and shape of the synthesized green Pd NPs. JEOL JEM 4000EX microscope Unit operating at 400 kV with a 0.12 nm resolution was nominated for this analysis. Scanning Electron Microscopy (SEM) was used for checking the scaffolds' morphological structure. Samples were fixed on the surface of aluminium stubs and coated with gold-palladium (max. of 20 kV) for further SEM investigation.

2.4.2. Crystalline phase by XRD

The crystalline nature and phase identification of the green synthesized Pd NPs were confirmed through the X-ray diffraction (XRD) technique. XRD Model smart lab (CuKα1 ¼ 1.5406 Å) has been used in this study. The analysis was carried out via Bruker Advanced D8 diffractometer with a monochromatic beam working at 200 mA and 45 kV in Bragg-Brentano geometry. XRD analysis was also evaluated for the prepared scaffolds to determine the effect of the doping process with green Pd NPS on the crystallinity structure of the scaffolds.

2.4.3. Vibrational properties (FTIR)

The Infrared technique was used for identifying the main functional groups in tested samples. Fourier transformed infrared analysis (FTIR; Nicolet Magna-IR 550 spectrometer, Madison, Wisconsin) was carried out for disks of 0.5 cm in diameter of the synthesized Alg/PVA/Pd NPs scaffolds. The samples were grounded with KBr and the sample bands were recorded within the measuring range of 400-4000 cm^{-1}.

2.4.4. Thermal investigation

Differential Scanning Calorimetry (DSC) is an investigation technique used for thermal properties studies of synthesized samples. It is used to detect the material transitions heat flow against the temperature. A prediction of the effect of PVA alginate and Pd NPs on the thermodynamic properties of the tested scaffold samples were observed. A Mettler Toledo DSC unit (STARe System, Schwerzenbach, Switzerland); modernized SETARAM labsys™ was used. DSC tests were carried out through heating 25 mg of the tested scaffolds at a flow rate of 2 °C/min in the range of 25–500 °C.

2.4.5. Mechanical properties

The mechanical properties of the synthesized hybrid scaffolds were done by detecting the Compressive Strength; Deformation Energy; Matrix Resilience and Rigidity Gradient. The scaffold samples were reshaped with a specific dimension of 10 × 5 × 5 mm^3 and compressed with a crosshead speed of 0.5 mm/min and a 1.0 kN load cell. A Textural Profile Analysis (TA.XTplus Texture Analyzer Stable Microsystems, Surrey, England) was used for different mechanical properties measurements.

2.5. Cell culture studies

2.5.1. Isolation and culture of human dental pulp stem cells (hDPSCs)

hDPSCs were extracted from three (one male and two females) healthy adult patients' sound third molars, which were recommended for extraction. Patients' teeth collections were carried out under the approved protocol by the Ethics Committee of the Faculty of Dentistry, Cairo University (approval number: 24/10/22). All the patients have completed a consent form before the collection process. The pulp of extracted teeth was enzymatically digested with collagenase type I (1 mg/ml) for a period of 20–40 min. Following that, standard cell culture conditions (37 °C, 5% CO_2) were used to grow the cells in Dulbecco's modified Eagle's medium (DMEM) supplemented with 1% penicillin-streptomycin (Pen-Strep), 20% fetal bovine serum (FBS), and 1% non-essential amino acids (All obtained from Gibco-Invitrogen, USA) (Ajlan et al., 2015).

2.5.2. Identification of hDPSCs

hDPSCs were distinguished as mesenchymal stem cells. This can be recognized through their morphology and plastic adherence. The fluorescent activated cell sorting (FACS) helps in the indication of hDPSCs via assessing the positive markers of $CD90^+$ and $CD44^+$ and the negative hematopoietic markers of $CD45^-$ and $CD34^-$ (AbuBakr et al., 2020; Soliman et al., 2022).

2.5.2.1. FACS analysis. FACS buffer (1 × phosphate-buffered saline (PBS), 5% FBS, 0.1% sodium azide) was used to wash hDPSCs (1.5 × 10^6), which were then diluted in 1.5 ml of PBS. Then, in the dark, we prepared and used FITC-conjugated mouse anti-human CD90, CD45, and CD34 and APC-conjugated mouse anti-human CD44 antibodies (BD Biosciences, USA). 100 μl of cells were combined with 10 μl of the matching antibody in each FACS tube and incubated for 30 min at 4 °C in the dark. Cellular marker expression was measured using a Becton Dickinson FACS Calibur Flow Cytometer (BD Biosciences, USA), and the data was processed using Cell Quest Pro Software Version 3.3 (BD Biosciences, USA) (Ajlan et al., 2015).

2.5.3. Biocompatibility of the constructed scaffolds

MTT assay was used to evaluate cell proliferation and growth. The vitality of the cells was assessed for the synthesized scaffolds after being in contact with hDPSCs for 72h. Individually, hDPSCs (1 × 10^4 cells) were cultured on cell culture slides (SPL, South Korea) with the constructed scaffolds, and anatomized with the synthesized scaffolds after 72 h. A cleaning process of the slides with PBS was carried out for 10min. in the dark with ethidium bromide/acridine orange (EB/AO; 100 μg/ml of each in 100 μl PBS). An examination process via fluorescence camera (Axio Imager Z2, Zeiss, Jena, Germany), and ZEN 11 blue version programming for Image Analysis (Zeiss, Jena, Germany) was done. The surviving, necrotic, early, and late apoptotic cells were photographed for every scaffold.

2.5.4. Osteogenic lineage induction

On 6-well plates, cells from the fourth passage were grown. Osteogenic differentiation was produced at 60–70% confluence using osteoinductive media made according to the technique of Vishnubalaji et al., 2012) et al. (Vishnubalaji et al., 2012). The DMEM medium was complemented by 1% Pen-Street, 10% FBS, 10 nM dexamethasone, and 10 mM glycerol phosphate disodium salt (β-glycerophosphate), 50 μg/ml L-ascorbic acid (Wako Chemicals GmbH, Germany) and 10 nM calcitriol (1α,25-dihydroxy vitamin D3) (Sigma, UK). Cells kept in the regular culture medium acted as controls. After 14 days, the ensuing osteogenesis was assessed using a quantitative real-time polymerase chain reaction to detect osteogenic gene expression (qRT-PCR).

2.5.5. Assessment of osteogenic genes

RT-PCR was used to identify total RNA-containing genes. QIAZOL was used to separate the RNAs (QIAGEN). cDNA was generated using an Applied Biosystems cDNA synthesis kit, and RT-PCR was done using an Applied Biosystems RT-PCR kit, using normal protocols. The RQ of each examined gene was assessed according to ΔΔCt. The RQ Calculation for target genes was achieved by $2^{-\Delta\Delta Ct}$ normalization to a housekeeping gene (Salem et al., 2021; Farag et al., 2022). Table 1 lists the primers that were investigated.

2.6. Co-culture of osteoblasts with PVA/Alg/Pd scaffolds

Sterilizing process for the synthesized scaffolds was done through UV irradiation for 30 min before cell seeding. 70% ethanol was added to the tested scaffold and maintained at room temperature for another 30 min. Osteoblasts with a cell density of (2 × 10^4) were seeded on the scaffolds (Hosseini et al., 2019).

Table (1)
Illustrates the utilized primers in the present work.

Gene	Accession	Primer (5′-3′)
RUNX2	NM_001015051.3	Forward: CATCTAATGACACCACCAGGC Reverse: GCCTACAAAGGTGGGTTTGA
OPN	NM_001040058.1	Forward: TGAAACGAGTCAGCTGGATGACCA Reverse: TGGCTGTGAAATTCATGGCTGTGG
GADPH	NM_002046.3	Forward: GAAGGTGAAGGTCGGAGTC Reverse: GAAGATGGTGATGGGATTTC

2.7. Scaffolds biocompatibility with osteoblasts using SEM

For osteoblasts co-cultured with PVA/Alg/Pd NPs scaffolds, scanning electron microscopy (SEM) analysis was performed (SEM Philips XL 20; FEI, Eindhoven, The Netherlands, at 20 KV, high vacuum mode). A 2% glutaraldehyde was added to the cacodylate buffer with 0.1M conc. For the cells fixation process at pH 7.4, all the samples were softly washed three times/20min. each, in 0.2M cacodylate buffer (pH 7.4) with 0.15M saccharose to protect the lipid structures. A post-fixation in 1% osmium tetroxide for 1h at room temperature was conducted. Two rapid changes of the earlier buffer and slowly dehydrated in increasing ethanol concentrations (from 25 to 100%, 15% per step). The samples were subsequently subjected to critical point drying (CPD) using liquid carbon dioxide, as per normal protocol (Mabrouk et al., 2022).

2.8. Statistical analysis

For all variables, the data were given as mean ± standard deviation. Analysis of variance (ANOVA) was used to compare groups, with T-tests used for different comparisons across groups. Statistical significance was defined as a P value of less than 0.05.

3. Results and discussion

3.1. Morphological structure (TEM and SEM analysis)

The green biosynthesis of Pd NPs was re-synthesized based on our previous report (Ismail et al., 2017a), via *Aspalathus linearis* natural plant extract. The formation of Pd NPs was confirmed via HR-TEM and XRD analysis. The HR-TEM results, Fig. 1 (a), revealed semi-spherical Pd NPs in the range of ~ 4–22 nm. The HR-TEM images also reveal the coating area surrounding the synthesized Pd NPs that may act as a stabilizing agent and decrease the NPs agglomeration. *Lin. Asp.* natural plant extracts reveal the phytochemical's vital effect as a reducing and chelating agent (Badeggi et al., 2020). The uncompleted shape similarity may attribute to the directing agent's strategies for the whole extract in the biosynthesizing process (Hirai et al., 2004; Long et al., 2010). Fig. 1 (b) is representing the selected area electron diffraction measurement (SAED), where it shows two main rings with intense spots indicating the poly-crystallinity nature of the biosynthesized Pd NPs. The rings are indexed as (111) and (200) reflections of the formation of the fcc Pd phase. The SAED results confirm the crystallinity nature of the biosynthesized NPs.

The SEM results for the tested scaffolds have shown an irregular interconnected porous structure. This is attributed to the freeze-dried process which caused a relative collapse in the polymer network. The interconnected pore structure could encourage water's diffusion through the hydrogel matrix. This confirms the vital role of the pore's connectivity in the fast swelling of the hydrogels. The SEM image, Fig. 1 (c and d) shows the morphology of the scaffolds, the PVA and Alg scaffolds mainly had irregular large pores structures. The results reveal a highly porous structure. However, the results showed a nonhomogeneous pore size with no common surface morphology. This may attribute to the different combinations between the PVA and Alg. Fig. 1 (e, f, and g) represents the SEM results of the doping effect with different Pd NPs concentrations. The scaffold sample of PVA/Alg loaded with 2Pd was characterized by an oriented lamellar porous structure and retained its shape for as long as necessary to complete the drying phase without pore collapse Fig. 1 (f). Doping with green synthesized Pd NPs positively assists in optimizing the density and the size of the scaffolds' pores. The pores should have a large size for PVA and Alg/PVA but a density that allowed interconnections among all the pores throughout the scaffold with Pd.

3.2. Crystallographic structure (XRD analysis)

Further XRD analysis was carried out to emphasize the phase, purity, and degree of crystallinity. Fig. 2 reveals the X-ray diffraction results for the prepared samples. The X-ray diffraction data confirmed the formation of pure palladium NPs phase, Fig. 2 (a). The XRD patterns detected two peaks at 40.4°, and 46.5° corresponding to the crystallography Bragg reflections of 111 and 200 reticular planes of face-centred cubic Pd Phase (Ismail et al., 2017a). This result agrees with the SAED data of the eco-friend synthesized Pd NPs represented in Fig. 1 b. The composite scaffolds before and after the inoculation of Pd NPs were assessed by X-ray diffraction. As can be noticed from Fig. 2(b) the native polymers; PVA, alginate, and alginate/PVA composite demonstrated semi-crystalline nature. The impregnation effect of Pd NPs does not

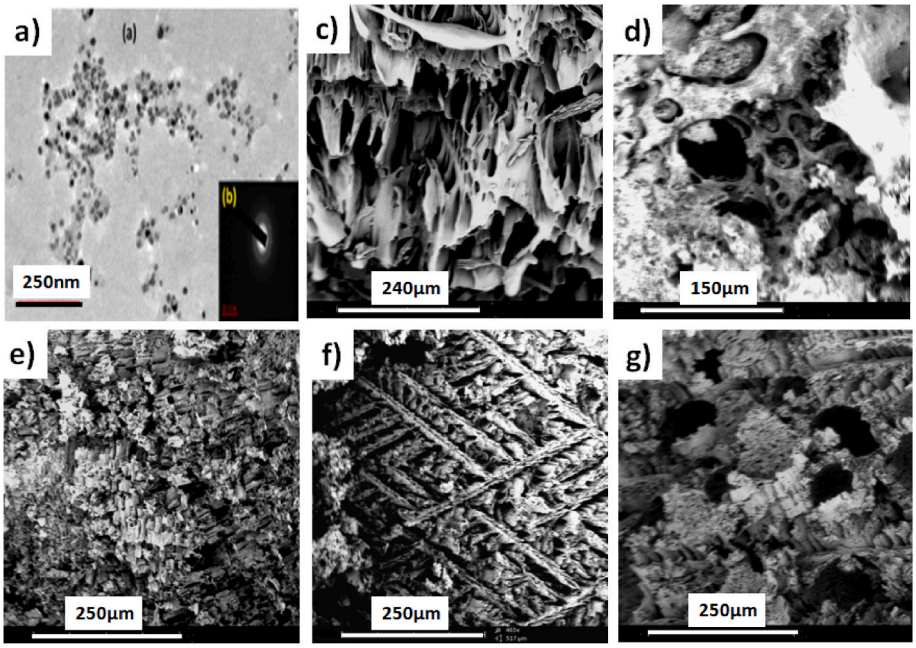

Figure (1). (a, b) representing the HR-TEM and SAED results for green Pd NPs; (c, d) representing the SEM images for the PVA and Alg. scaffolds, respectively; (e, f, and g) representing the Pd NPs different concentrations effect.

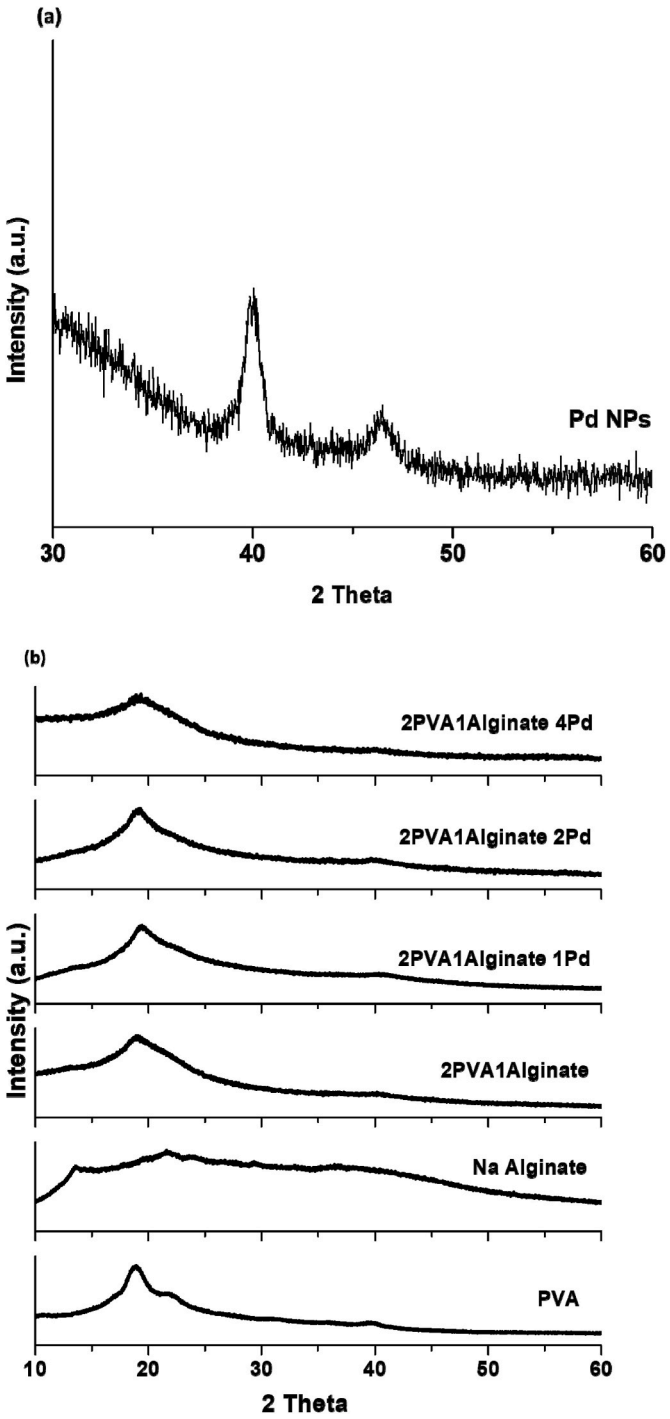

Figure (2). The XRD results of a) Pd NPs and b) Pd NPs impregnated within the polymer composite.

affect the crystallinity nature degree of PVA/Alg nanocomposite. The crystallography Bragg peaks of the Pd NPs were not clear in the synthesized scaffolds which may attribute to low Pd NPs concentration. However, the vital effect of the doping process with Pd NPs has been reported in other analysis tests.

3.3. Vibrational properties (FTIR analysis)

The spectra of FTIR of the prepared composite scaffolds inserted with various ratios of Pd NPs are represented in Fig. 3. The functional groups of the native polymers, PVA and Alg were assessed to other fabricated

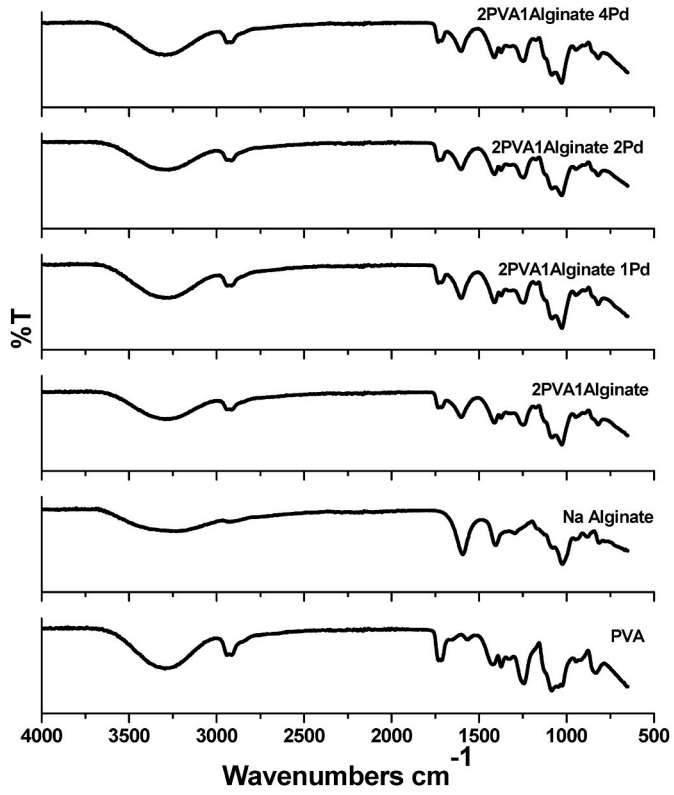

Figure (3). FTIR spectra of pure PVA; Na Alginate; PVA/Alg scaffold; and the scaffolds loaded with various ratios of green Pd nanoparticles.

composite scaffolds. The spectrum of FTIR of the PVA sample showed various characteristic peaks of modes of vibrational. The characteristic peaks at 3291, 2913, and 1432 cm^{-1} belong to the presence of stretching mode of the hydroxyl group (-OH), symmetric CH_2 stretching, and –bending CH_2 bands, respectively. The peak at 1318 cm^{-1} is allocated to the bending hydroxyl (-OH) group and the vibration mode of the CH group. 1087, 922, and 840 cm^{-1} bands attributed to the C=O mode of stretching, CH_2 bending, and CH mode, respectively. The characteristic peak of 3283 cm^{-1} is attributed to the stretching OH band, while the peak at 2929 cm^{-1} belongs to the CH vibration mode of stretching of the methylene structure. The peaks at 1085 cm^{-1} belonging to the (C–O–C) vibration mode of stretching were also noted. The band at 1407 cm^{-1} was assigned to the carboxylate (C=O) vibration mode of stretching (Han et al., 2013). Within the alginate molecule, the polyglycolic acid residue is observed in a chelating structure in which Ca^{2+} and polymannuronic acid residues are reacted (Han et al., 2013). The FTIR spectra of the PVA/alginate sample reveal a wide band at (3655-2977 cm^{-1}) attributed to the O–H vibration mode of the stretching band. Additional three main strong peaks at 1596; 1410 and 1016 cm^{-1} belong to NH_2 or C=C vibration mode of stretching; C–H and –C–O group, respectively (Luo et al., 2017; Li et al., 2017; Da Silva et al., 2016; Ismail et al., 2017b; Mostafa et al., 2014).

Very small vibrational bands allocated at 1099, 877, and 817 cm^{-1} may be assigned to –C–O–C vibration mode of stretching, C–H vibration mode of bending, and C–O, respectively (Sudhamani et al., 2003; Prasad, 2014). A clear decrease in the peak intensity in the PVA/Alg sample is observed, due to the reaction between the used polymers. Also, the FT-IR spectrum of the PVA/Alg nanocomposite loaded with Pd NPs revealed a slight intensity enhancement compared to PVA/Alg composite. This is indicated by the loading process with the green eco-friendly synthesized Pd on a nanoscale. All the characteristic vibrational bands were represented with no obvious shift indicating the physical mechanism-oriented adsorption process (Yang et al., 2018).

3.4. Thermal behaviour investigation (DSC analysis)

A thermal behavior study for the synthesized PVA/Alg/Pd scaffolds was done via Differential Scanning Calorimetry and represented in Fig. 4. The DSC curve of pure PVA polymer reveals weight loss up to ~180 °C attributed to evaporation of water (Mostafa et al., 2009; Reguieg et al., 2020). There is an endothermic peak in the range of 295–363 °C due to the transition temperature of the glass phase (T_g) of the polymer electrolytes (Sudhamani et al., 2003). The endothermic peak of pure PVA represents a melting temperature (T_m) at 324 °C. While the PVA alginate hybrid sample curve reveals a melting temperature of 286 °C. The decrease in the melting point is attributed to the molecular interaction between the PVA polymer and sodium alginate. Furthermore, an exothermic peak at 237 °C in Na alginate DSC data was shifted to 247 °C in the PVA alginate hybrid sample curve confirming the interaction effect of PVA on the melting temperature. The exothermic peak is ascribed to biopolymer degradation. On the other hand, there are three endothermic peaks at ~107 °C, ~245 °C, and ~472 °C for the DSC curve of green synthesized Pd NPs. The first peak is belonged to the evaporation of water, while the second and third ones are attributed to the part and completed oxidation procedure of Pd NPs into the palladium oxide phase (PdO) (Ismail et al., 2017a). The incorporation of Pd NPs into hybrid PVA/alginate samples shows a slight effect on the endothermic peak representing the polymer degradation melting point as shown in Table 2. The results reveal an inverse relationship between T_m and Pd concentration i.e., by increasing Pd NPs concentration in the hybrid scaffold samples, the melting temperature value (T_m) decreases.

3.5. Evaluation of the mechanical properties

The mechanical properties are carried out for the synthesized PVA/Alg/Pd scaffolds. The investigated mechanical properties are such as Compressive Strength (CS), Rigidity Gradient (RG), Deformation Energy (DE), and Matrix Resilience (MR). The Pd NPs have been added to the prepared PVA Alg composite in different concentrations as reported in the scaffolds preparation process. Proportions of 0.5, 1.5, 2.5, and 3.5 wt %, were added followed by mechanical mixing for 30 min. A pure PVA sample (i.e., 0 wt% Pd NPs) was used as the control sample. Fig. 5 represents the mechanical properties of the synthesized scaffolds. The CS, DE, and RG (%) of all the prepared PVA/Alg/Pd scaffolds were compared to PVA and PVA alginate as shown in Fig. 5 (a, b, and d). The CS, DE, and RG (%) data clearly indicate a proportional increase with the increase of Pd NPs concentration in the scaffolds. The data reveal increasing in the CS values from 43 MPa to 52 MPa for PVA/Alg/1Pd scaffolds and PVA/Alg/4Pd scaffolds, respectively. Likewise, CS values and DE results also show an increasing record from 278 J/m^3 to 394 J/m^3 with increasing the Pd NPs ratio in the prepared composite scaffolds. Furthermore, RG data was clearly showing a proportional increase from 35.3Pa to 74.3Pa integration with the increase of Pd NPs ratio. In contrast, the MR of the PVA/Alg/1Pd scaffolds decreased from 0.94 to 0.71 for the composite scaffold PVA/Alg/4Pd, as shown in Fig. 5 (c). Generally, the resilience results show a decrease in the composite scaffold PVA/Alg/Pd value as compared to the initial MR value of PVA and PVA/Alg results. In conclusion, the doping process with metallic Pd NPs aided in the augmentation of numerous mechanical properties for the prepared composite scaffolds. The mechanical data confirmed the favorable effect of loading with the green synthesized Pd NPs and their concentration. Enhancing the various mechanical properties of the synthesized scaffolds is essential for further bone tissue engineering applications.

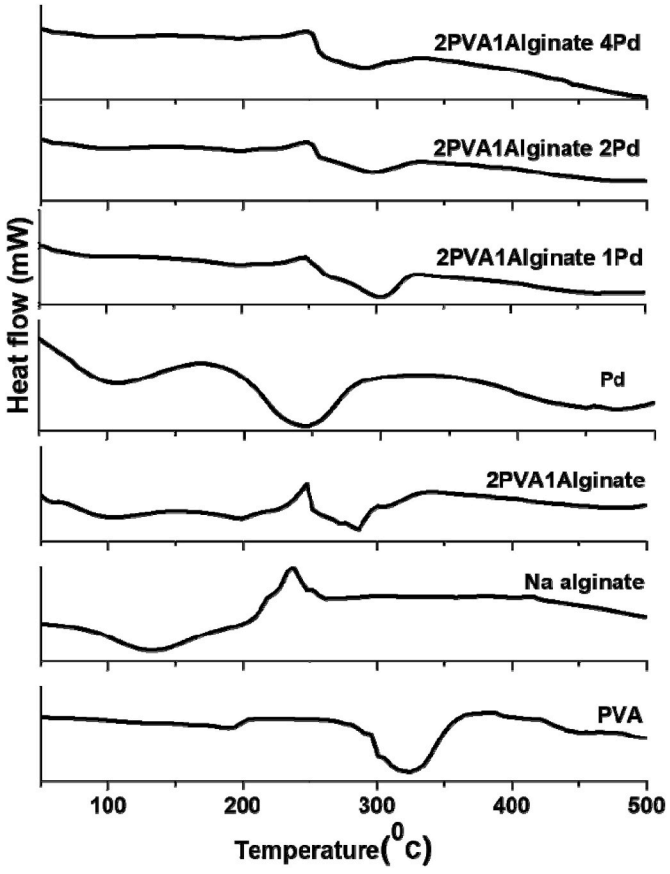

Figure (4). The DSC thermograms of PVA; alginate; PVA/Alg; Pd NPs and the composite of Pd NPs concentrations.

Table (2)
Thermal DSC characteristics of PVA/Alg/Pd NPs scaffold samples.

Samples	T_o	T_m	T_c	Range (T_c-T_o)
PVA	295	324	363	68
2PVA/1Alg	252	286	329	77
PVA/Alg/1Pd	261	305	324	63
PVA/Alg/2Pd	261	300	324	63
PVA/Alg/4Pd	261	290	324	63

T_o onset, T_m melting peak, Tc melting completion temperatures.

3.6. In vitro cell culture studies

3.6.1. hDPSCs recognition

hDPSCs were successfully isolated and proliferated. They reveal a characteristic spindle-shaped morphology as represented in (Fig. 6 (a)). FACS analysis revealed positive CD90 and CD44 markers of the hDPSCs, (Fig. 6 (b)). The Figure also represented the negative hematopoietic markers for CD34 and CD45. This agrees with previous studies which reported the positive stromal cell-associated marker expression and the negative hematopoietic and endothelial marker expression of the hDPSCs (Ajlan et al., 2015; Kamel et al., 2020).

3.6.2. Biocompatibility of the various composite scaffolds with hDPSCs

MTT assay was used to evaluate scaffold biocompatibility and measure cell proliferation and growth (Mahdi et al., 2019). Fig. 7 reveals the percentage of cells' proliferation assessed after the constructed scaffolds were subjected to hDPSCs for 72h. The constructed scaffolds retained the cell viability (survival percentage) throughout the 72h cells incubation: 83.588%, 77.396%, 94.78%, 131.662%, and 159.2% for PVA, PVA/Alg, PVA/Alg/1Pd, PVA/Alg/2Pd, and PVA/Alg/4Pd scaffolds respectively. At a p-value of 0.05, statistical studies using ANOVA showed a difference between cells' viability on the various scaffolds. After being in contact with hDPSCs for 72h, the vitality of the cells was assessed for the synthesized scaffolds, and their matching fluorescent pictures, are shown in Fig. 8 where the control cells (hDPSCs) showed

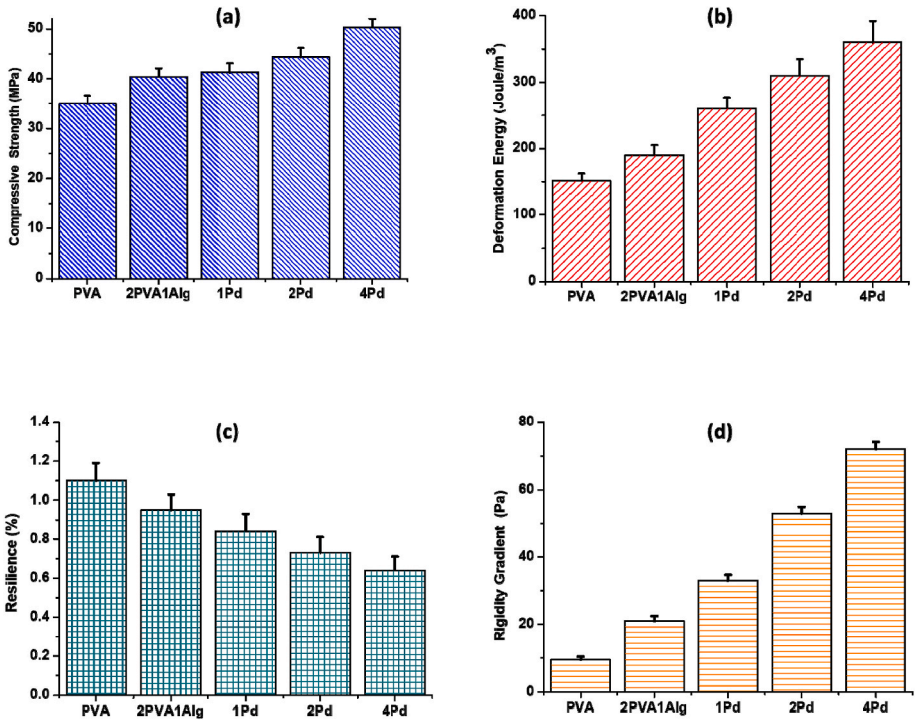

Figure (5). Physico-mechanical properties of the prepared scaffolds represented by (a) compressive strength; (b) deformation energy; (c) matrix resilience and (d) rigidity Gradient.

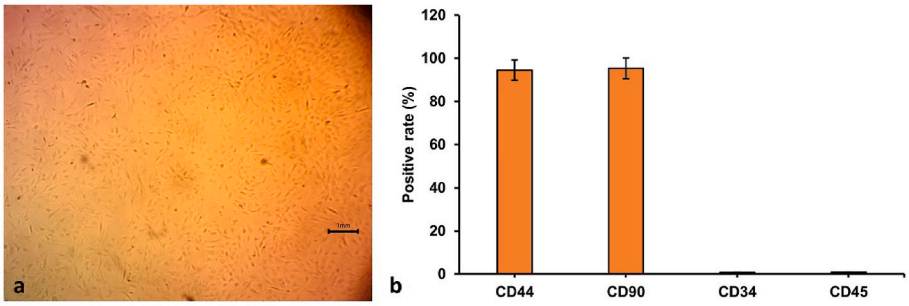

Figure (6). Demonstrates a) hDPSCs in culture and b) FACS analysis of hDPSCs, positive for $CD44^{+}$ (94.48%) & $CD90^{+}$ (95.34%) & negative for $CD34^{-}$ (0.686%) & $CD45^{-}$ (0.892%).

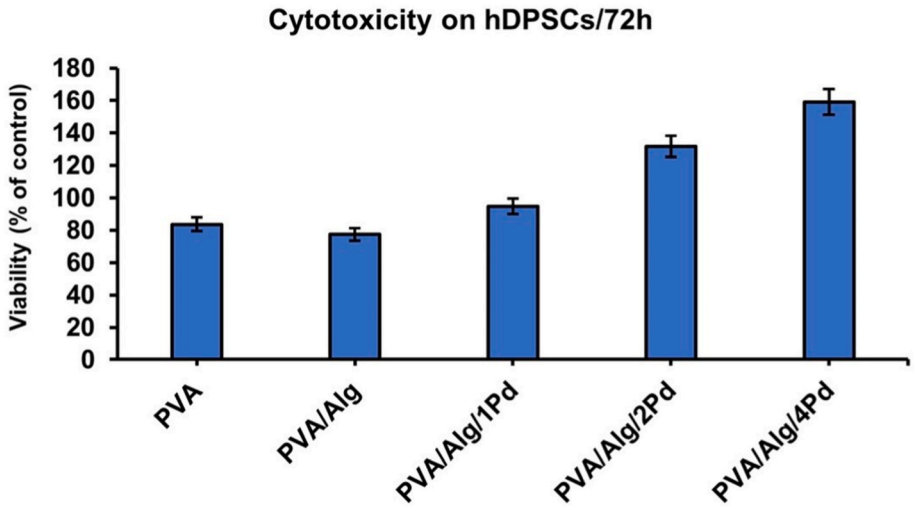

Figure (7). Cells' proliferation (%) assessed after subjecting the fabricated scaffolds to hDPSCs for 72h.

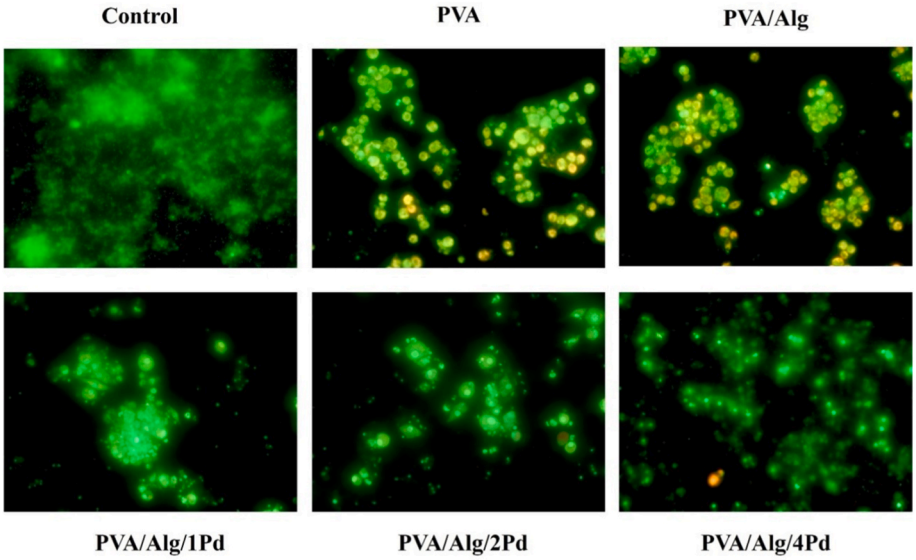

Figure (8). Fluorescence images after 72h of exposure of the constructed scaffolds to hDPSCs. (viable cells: dark green, early apoptotic: light green, late apoptotic: gold, necrotic: orange).

the highest surviving cells reflected as dark green fluorescent color followed by PVA/Alg/4Pd, PVA/Alg/2Pd, PVA/Alg/1Pd scaffolds respectively. However, the early apoptotic cells appeared as light green fluorescent colors, late apoptotic cells as a goldy fluorescent color, and necrotic cells appeared to have an orange color and were observed in PVA/Alg and PVA scaffolds. This shows that the scaffolds are very well biocompatible with the cells. This agrees with Kim et al., 2020 (Kim et al., 2020), who reported the absence of cell lysis or toxicity caused by the PVA/gelatine hydrogels and suggested that they are clinically safe and effective. Moreover, when Pd NPs were added to PVA/Alg scaffolds, the biocompatibility of the Pd nanocomposite scaffolds was significantly higher than the pure PVA and PVA/Alg scaffolds. This confirmed the affectivity of Pd NPs in the biocompatibility enhancement of PVA/Alg scaffolds. In this regard, greater cell survival depends on the optimal incorporation of Pd NPs into the nanocomposite scaffolds. Pd has high potential features in biomedicine, where it is frequently utilized in surgical equipment and dental products (Azizi et al., 2021).

3.6.3. *Osteogenic lineage induction*

In the present study, hDPSCs were differentiated into osteoblasts. This is in accordance with Vishnubalaji et al., 2012 (Vishnubalaji et al., 2012), who reported that cells that underwent osteogenic induction by the same approach and displayed enhanced ALP staining when compared to negative control cells.

3.6.4. *qRT-PCR results*

To analyze the osteogenic activity of the differentiated osteoblasts, we speculated that differentiated cells showed active expression of *Runx-2* and *Osteopontin* genes. As a result, we used qRT-PCR to examine the mRNA levels of their expression. The T-test revealed a substantial increase ($p < 0.05$) in gene expression of *Runx-2* and *Osteopontin* in osteoblasts compared to undifferentiated dental pulp stem cells (Fig. 9). This is consistent with past research where the mRNA gene expression of *Runx-2* and *Osteopontin* was regarded as a crucial tool for displaying osteogenesis, in which upregulation of these osteogenic markers indicated a successful osteogenic differentiation (Hosseini et al., 2019; Jiménez et al., 2018).

3.7. *Scaffolds biocompatibility with the induced osteoblasts using SEM*

Seeded scaffolds were photographed using SEM after 7 days of

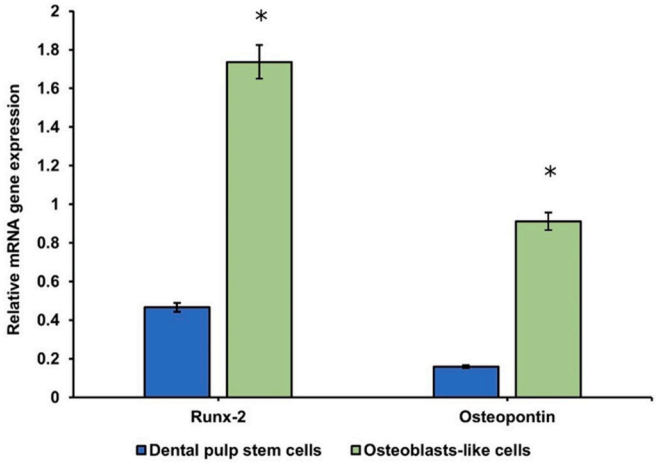

Figure (9). A diagram showing the qRT-PCR results of *Runx-2* and *Osteopontin* gene expression. The results are expressed as mean ± SD using a T-test at p-value< 0.05.

culture to evaluate if the scaffolds' mean pore size influenced cell shape (Xiang et al., 2021; Pedram et al., 2021). A uniform and homogenous distribution of cells were observed after seeding the osteoblasts on the prepared scaffolds for 7 days, especially the scaffolds including Pd NPs. The cells were found to have a phenotypically flat shape (Fig. 10). However, in the SEM examination of the scaffold when adding alginate with PVA, the hDPSCs showed necrotic cells with a high distribution of bone-like apatite crystals denoting that this scaffold failed to attach cells (Fig. 10 (c & d)). In scaffolds doped with Pd NPs, hDPSCs are represented as organized multi-layer and overlapping layers, respectively. In this study, the TEM and SEM results for the tested scaffolds revealed an interconnected high porous structure with nonhomogeneous pore size. The SEM images showed how the cells penetrated these pores. Moreover, cells appear with a regular shape with high cell density (Fig. 10 (e–j)), indicating that the scaffolds with Pd NPs offered appropriate mechanical support and stability to the cultured cells and increased their viability. It could be hypothesized that Pd NPs increase cell viability as green synthesized Pd NPs positively assist in optimizing the density and the size of the scaffolds' pores that allowed interconnections among all

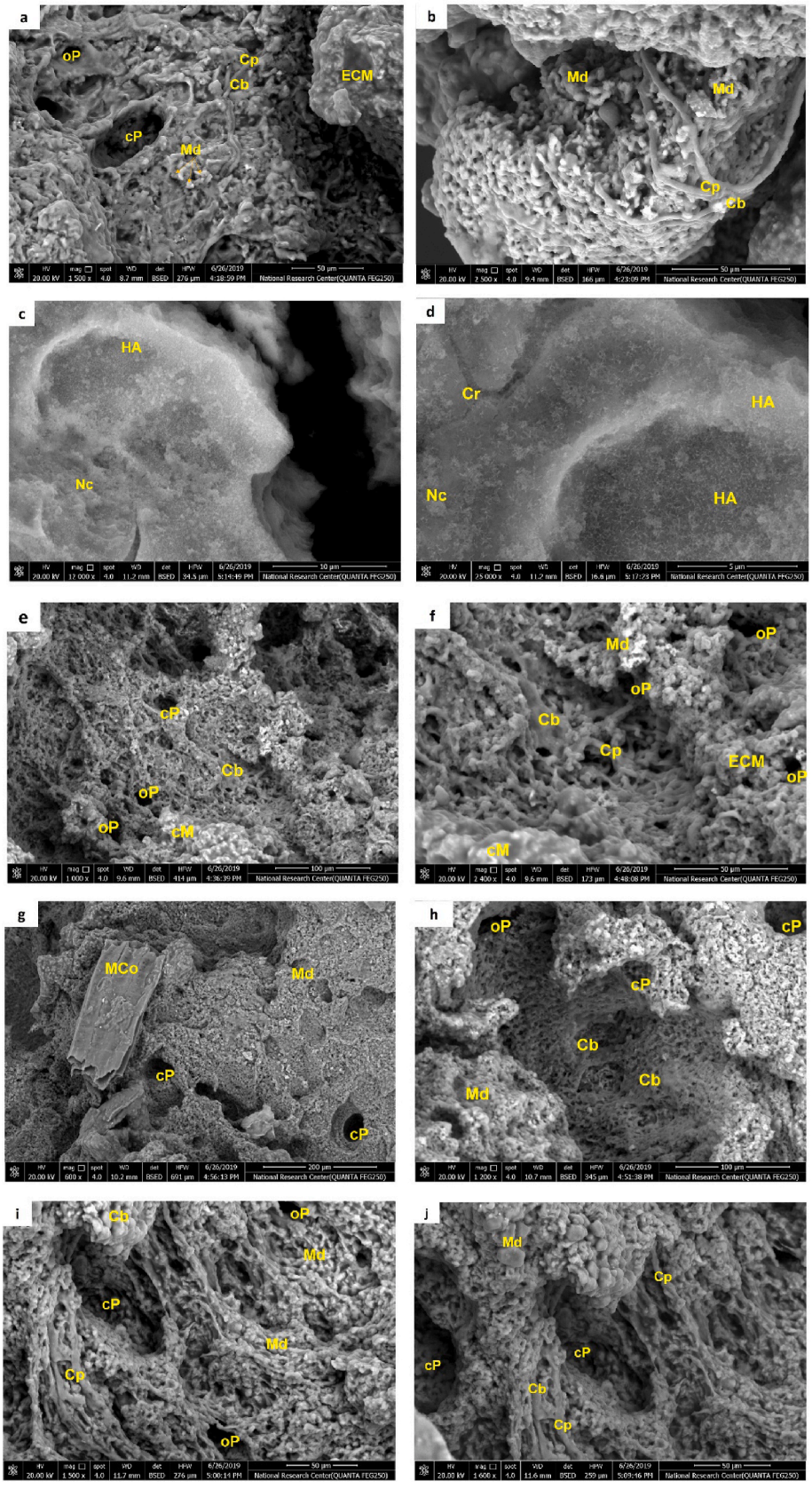

Figure(10). Scanning electron micrographs of differentiated osteoblasts after seeding for 7 days on PVA scaffold showing:**(a)** ECM, collagen with numerous cell processes attached to the surrounding matrix, open and closed pores **(a& b)** apparent flattened cell body with numerous cell processes, mineral deposits; PVA/Alg scaffold showing: **(c & d)** apparent mineralization with hydroxyapatite crystals and some necrotic cells **(d)** crack filled with collagen bridges in between the mineralized scaffold; PVA/Alg loaded with 1Pd scaffold showing: **(e & f)** differentiated cells with apparent flattened cell bodies, opened and closed pores and collagenous membrane extending above the scaffold with extracellular matrix in between the cell processes **(f)** mineral deposits (bone nodules) and extracellular matrix; PVA/Alg loaded with 2Pd scaffold showing: **(g)** highly mineralized collagen, mineral deposits (bone nodules) and closed pores **(h)** cell bodies with extracellular matrix in between them, opened and closed pores and mineral deposits; PVA/Alg loaded with 4Pd scaffold showing: **(i & j)** cells with apparent flattened cell body and numerous cell processes, mineral deposits upon the matrix (bone nodules) and in between the cell processes; opened and closed pores. [Cb: cell body, Cp: cell processes, cP: closed pore, oP: opened pore, ECM: extracellular matrix, Md: mineral deposits, HA: Hydroxyapatite nanocrystals, Nc: necrotic cell, Cr: crack-filled with collagen bridges, cM: collagenous membrane covered with mineral deposits, Mco: mineralized collagen].

the pores throughout the scaffolds. The porosity and pore size of biomaterial scaffolds play a critical role in bone formation in vitro and in vivo as they enhance migration and cell transport. They also affect the vascularization of the newly formed bone tissue (Karageorgiou and Kaplan, 2005). In the presence of Pd NPs, the extracellular matrix was produced, and mineralized nodules were formed. This is consistent with the study of Bellows et al. 1986, in which the cells were cultivated until they produced multilayers with nodules. Mineralization was discovered only after the creation of the nodules.

4. Conclusions

In the current work, innovative hybrid scaffolds of polyvinyl alcohol/alginate (PVA/Alg) composite loaded with different palladium nanoparticle concentrations (Pd NPs) have been successfully synthesized. The Pd NPs were greenly synthesized via *Asp. Lin.* natural plants extract. The Pd NPs have been used to enhance the different properties of the pure PVA/alginate scaffolds for further biomedical applications. The PVA/Alg scaffold loaded with Pd is characterized by an oriented lamellar porous structure and retained its shape for as long as necessary to complete the drying phase without pore collapse. The results reveal the positive effect of doping with green synthesized Pd NPs in optimizing the density and the size of the scaffolds' pores. The effect of the metallic doping process on the crystallinity nature of the synthesized scaffolds was not clear, which may be attributed to the low Pd NPs concentrations. However, the doping process with Pd NPs concentrations revealed a noticeable enhancement in various mechanical properties of the synthesized scaffolds. The CS, DE, and RG (%) data show a proportional increase as the concentration of Pd NPs in the scaffolds increases. The positive impact of loading with the green synthesized Pd NPs and their concentration was supported by the mechanical data. This enhancement is essential for tissue engineering applications. The human dental pulp stem cells (hDPSCs) were successfully isolated and proliferated. The MTT assay revealed a great enhancement in the biocompatibility features of the PVA/Alg/Pd nanocomposite scaffolds in comparison to the pure PVA and PVA/Alg scaffolds. The SEM images reveal a uniform and homogenous distribution of osteoblasts on the prepared scaffolds. The results confirmed that Pd NPs scaffolds offered appropriate mechanical support and stability to the cultured cells.

Funding

E.I. would like to thank and acknowledge the national research foundation (NRF) for their support through the postdoctoral fellowship, grant Number: 138514.

CRediT authorship contribution statement

Enas Ismail: Writing – review & editing, Writing – original draft, Visualization, Methodology, Formal analysis, Conceptualization. **Mostafa Mabrouk:** Writing – review & editing, Project administration, Methodology, Data curation, Conceptualization. **Zeinab A. Salem:** Writing – review & editing, Resources, Investigation, Funding acquisition. **Nermeen AbuBakr:** Writing – review & editing, Methodology, Investigation, Data curation. **Hanan Beherei:** Writing – review & editing, Validation, Resources, Funding acquisition.

Declaration of competing interest

The authors declare that they have no known competing financial interests or personal relationships that could have appeared to influence the work reported in this paper.

Data availability

No data was used for the research described in the article.

References

AbuBakr, N., Haggag, T., Sabry, D., Salem, Z.A., 2020. Functional and histological evaluation of bone marrow stem cell-derived exosomes therapy on the submandibular salivary gland of diabetic Albino rats through TGFβ/Smad3 signaling pathway. Heliyon 6 (4), e03789.

Ahmadi, S., Rabiee, N., Rabiee, M., 2019. Application of Aptamer-based hybrid molecules in early diagnosis and treatment of diabetes mellitus: from the concepts towards the future. Curr. Diabetes Rev. 15, 309–313.

Ajlan, S.A., Ashri, N.Y., Aldahmash, A.M., Alnbaheen, M.S., 2015. Osteogenic differentiation of dental pulp stem cells under the influence of three different materials. BMC Oral Health 15, 132, 2015.

Azizi, F., Heidari, F., Ghaedi, M., 2021. Mechanical properties and biocompatibility ofHydroxyapatite/manganese dioxide/palladium nanocomposite scaffolds filled by natural chitosan. Adv. Ceramic. Progress. 7 (3), 1–9.

Badeggi, U., Ismail, E., Adeloye, A., et al., 2020. Green synthesis of gold nanoparticles capped with procyanidins from leucosideasericea as potential ant*idiab*etic and antioxidant agents. Biomolecules 10 (3), 452.

Bellows, C.G., Aubin, J.E., Heersche, J.N.M., Antosz, M.E., 1986. Mineralized bone nodules formed in vitro from enzymatically released rat calvaria cell populations. Calcif. Tissue Int. 38, 143–154.

Brierly, G.I., Tredinnick, S., Lynham, A., Woodruff, M.A., 2016. Critical sized mandibular defect regeneration in preclinical in vivo models. Curr. Mol. Biol. Rep. 2, 83–89.

Da Silva, A., Macedo, T., Coletta, D., Feldman, S., Pereira, M., 2016. Synthesis, characterization, and cytotoxicity of Chitosan/Polyvinyl alcohol/bioactive glass hybrid scaffolds obtained by Lyophilization. Rev. Mater. 21 (4), 964–973.

d'Aquino, R., Papaccio, G., Laino, G., Graziano, A., 2008. Dental pulp stem cells: a promising tool for bone regeneration. Stem Cell Rev. 4 (1), 21–26.

Farag, D.B., Yousry, C., Al-Mahallawi, A.M., El-Askary, H.I., Meselhy, M.R., AbuBakr, N., 2022. The efficacy of Origanum majorana nanocubosomal systems in ameliorating submandibular salivary gland alterations in streptozotocin-induced diabetic rats. Drug Deliv. 29 (1), 62–74.

Gombotz, W.R., Wee, S.F., 2012. Protein release from alginate matrices. Adv. Drug Deliv. Rev. 64, 194–205.

Han, Y., Zeng, Q., Li, H., Chang, J., 2013. The calcium silicate/alginate composite: preparation and evaluation of its behavior as bioactive injectable hydrogels. Acta Biomater. 9 (11), 9107–9117.

He, C., Heidari Majd, M., Shiri, F., Shahraki, S., 2021. Palladium and platinum complexes of folic acid as new drug delivery systems for treatment of breast cancer cells. J. Mol. Struct. 1229, 129806.

Hirai, N., et al., 2004. Characteristics of the absorption and the emission of hydrogen in palladium nanoparticles encapsulated into graphite at 1.0 MPa hydrogen pressure. Sci. Technol. Adv. Mater. 5 (1–2), 181–185.

Hosseini, F.S., Enderami, S.E., Hadian, A., Abazari, M.F., Ardeshirylajimi, A., Saburi, E., Soleimanifar, F., Nazemisalman, B., 2019. Efficient osteogenic differentiation of the dental pulp stem cells on β-glycerophosphate loaded polycaprolactone/polyethylene oxide blend nanofibers. J. Cell. Physiol. 234 (8), 13951–13958.

Ismail, E., Khenfouch, M., Dhlamini, M., Dube, S., Maaza, M., 2017a. Green palladium and palladium oxide nanoparticles synthesized via Aspalathus linearis natural extract. J. Alloys Compd. 695, 3632–3638.

Ismail, E., Kenfouch, M., Dhlamini, M., Dube, S., Maaza, M., 2017b. Green biosynthesis of Rhodium nanoparticles via AspalathusLinearisnatural extract. J. Nanomater. Mol. Nanotechnol. 6 (2), 1–7.

Jang, J.W., Yun, J.H., Lee, K.I., et al., 2012. Osteoinductive activity of biphasic calcium phosphate with different rhBMP-2 doses in rats, 4. In: Oral Surgery, Oral Medicine, Oral Pathology and Oral Radiology, 113, pp. 480–487.

Jiménez, N.T., Munévar, J.C., González, J.M., Infante, C., Lara, S.J., 2018. In vitro response of dental pulp stem cells in 3D scaffolds: a regenerative bone material. Heliyon 4 (9), e00775.

Kamel, A.H., Kamal, S.M., AbuBakr, N., 2020. Effect of smoking on the proliferation capacity and osteogenic potential of human dental pulp stem cells (DPSCs). Dental Med. Problem. 57 (1), 19–24.

Karageorgiou, V., Kaplan, D., 2005. Porosity of 3D biomaterial scaffolds and osteogenesis. Biomaterials 26 (27), 5474–5491.

Kiani, M., Rabiee, N., Bagherzadeh, M., Ghadiri, A.M., Fatahi, Y., Dinarvand, R., Webster, T.J., 2020. High-gravity-assisted green synthesis of palladium nanoparticles: the flowering of nanomedicine. Nanomed. Nanotechnol. Biol. Med. 30, 102297.

Kim, S., Lim, H., Kim, S., Lee, D.Y., 2020. Effect of PVA concentration on strength and cell growth behavior of PVA/gelatin hydrogels for wound dressing. J. Biomed. Eng. Res. 41 (1), 1–7.

Krafczyk, N., Glomb, M.A., 2008. Characterization of phenolic compounds in rooibos tea. J. *Agric. Food Chem.* 56, 3368–3376.

Lee, K.Y., Mooney, D.J., 2012. Alginate: properties and biomedical applications. Prog. Polym. Sci. 37 (1), 106–126.

Li, X., Jiang, Y., Wang, F., Fan, Z., Wang, H., Tao, C., Wang, Z., 2017. Preparation of polyurethane/polyvinyl alcohol hydrogel and its performance enhancement via compositing with silver particles. RSC Adv. 7 (73), 46480–46485.

Lindroos, B., Mäenpää, K., Ylikomi, T., Oja, H., Suuronen, R., Miettinen, S., 2008. Characterisation of human dental stem cells and buccal mucosa fibroblasts. Biochem. Biophys. Res. Commun. 368 (2), 329–335.

Long, V.N., et al., 2010. Chemical synthesis and characterization of palladium nanoparticles. Adv. Nat. Sci. Nanosci. Nanotechnol. 1 (3), 035012.

Luo, Y., Luo, G., Gelinsky, M., Huang, P., Ruan, C., 2017. 3D bioprinting scaffold using alginate/polyvinyl alcohol bioinks. Mater. Lett. 189, 295–298.

Mabrouk, M., Ismail, E., Beherei, H., Abo-Elfadl, M.T., Salem, Z.A., Das, D.B., AbuBakr, N., 2022. Biocompatibility of hydroxyethyl cellulose/glycine/RuO_2 composite scaffolds for neural-like cells. Int. J. Biol. Macromol. 209, 2097–2108.
Mahdi, Z., Saeed, S., Sara, A., Kadhim, A., 2019. Synthesis and characterization of porous cytocompatible scaffolds from polyvinyl alcohol-chitosan. Bull. Mater. Sci. 42 (1), 1–9.
Marthy, S., Richter, M., 1998. Human immunodeficiency virus activity in rib allografts. J. Oral Maxillofac. Surg. 56 (4), 474–476.
Mostafa, A.A., Oudadesse, H., Mohamed, M.B., Foad, E.S., Le Gal, Y., Cathelineau, G., 2009. Convenient approach of nanohydroxyapatite polymeric matrix composites. Chem. Eng. J. 153, 187–192.
Mostafa, A., Oudadesse, H., El Sayed, M.H., Kamal, G., Kamel, M., Foad, E., 2014. Kinetic evaluation study on the bioactivity of silver doped hydroxyapatite-polyvinyl alcohol nanocomposites. J. Biomed. Mater. Res. 102 (12), 4609–4615.
Pedram, I., Mohammad, G., Abbasali, K., Mohammad, D., Mehran, Naif A., Mehran, H., Ramin, M., Saeed, S., Davood, T., Afrasyab, K., 2021. Bioprinting of three-dimensional scaffold based on alginate-gelatin as soft and hard tissue regeneration. J. Mater. Res. Technol. 14, 2853–2864.
Phan, T., Huynh, T., Manivasagan, P., Mondal, S., Oh, J., 2020. An up-to-date review on biomedical applications of palladium nanoparticles. Nanomaterials 10 (66), 1–6.
Pittenger, M.F., Mackay, A.M., Beck, S.C., et al., 1999. Multilineage potential of adult human mesenchymal stem cells. Science 284 (5411), 143–147.
Prasad, R., 2014. Synthesis of silver nanoparticles in photosynthetic plants. J. Nanopartic. 1–8.
Reguieg, F., Ricci, L., Bouyacoub, N., Belbachir, M., Bertoldo, M., 2020. Thermal characterization by DSC and TGA analyses of PVA hydrogels with organic and sodium MMT. Polym. Bull. 77, 929–948.
Ruedinger, F., Lavrentieva, A., Blume, C., Pepelanova, I., Scheper, T., 2015. Hydrogels for 3D mammalian cell culture: a starting guide for laboratory practice. Appl. Microbiol. Biotechnol. 99, 623–636.
Salem, Z.A., Kamel, A.H., AbuBakr, N., 2021. Salivary exosomes as a new therapy to ameliorate diabetes mellitus and combat xerostomia and submandibular salivary glands dysfunction in diabetic rats. J. Mol. Histol. 52 (3), 467–477.
Shanthi, K., Vimala, K., Gopic, D., Kannan, S., 2015. Fabrication of a pH-responsive DOX conjugated PEGylated palladium nanoparticle mediated drug delivery system: an in vitro and in vivo evaluation. RSC Adv. 5, 44998–45014.
Soliman, T., Ali, Z., Zayed, M., Sabry, D., AbuBakr, N., 2022. Assessing the bone-healing potential of bone marrow mesenchymal stem cells in jawbone osteoporosis in albino rats. Dental Med. Problem. 59 (1), 75–83.
Sordi, M.B., Ariadne, M.C., Fredel, R., Magini, P.T., 2021. Sharpe, "Three-dimensional bioactive hydrogel-based scaffolds for bone regeneration in implant dentistry". Mater. Sci. Eng. C 124, 112055.
Sudhamani, R., PrasadK, M., Udaya, S., 2003. DSC and FTIR studies on Gellan and polyvinyl alcohol (PVA) blend films. Food Hydrocolloids 17 (3), 245–250.
Tatullo, M., Marrelli, M., Shakesheff, K.M., White, L.J., 2015. Dental pulp stem cells: function, isolation, and applications in regenerative medicine. J Tissue Eng Regen Med 9, 1205–1216.
Treenate, P., Monvisade, P., 2017. Crosslinker effects on properties of hydroxyethyl acryl chitosan/sodium alginate hydrogel films. Macromol. Symp. 372 (1), 147–153.
Vishnubalaji, R., Al-Nbaheen, M., Kadalmani, B., Aldahmash, A., Ramesh, T., 2012. Comparative investigation of the differentiation capability of bone-marrow- and adipose-derived mesenchymal stem cells by qualitative and quantitative analysis. Cell Tissue Res. 347 (2), 419–427.
Xiang, Li, Saber-Samandari, S., Mohsen Heydari, B., Mohammad Reza, M., Sajad Niazi, A., Davood, T., Amirsalar, K., Afrasyab, K., 2021. Experimental measurement and simulation of mechanical strength and biological behavior of porous bony scaffold coated with alginate-hydroxyapatite for femoral applications. Compos. Sci. Technol. 214, 108973.
Yang, X., Zhou, T., Ren, B., Hursthouse, A., Zhang, Y., 2018. Removal of Mn (II) by sodium alginate/graphene oxide composite double-network hydrogel beads from aqueous solutions. Sci. Rep. 8 (1), 1–16.